


## Spectral characterization of the Rashba spin-split band in a lead halide perovskite single crystal by photocurrent heterodyne interference spectroscopy

Yoshihiro Ogawa<sup>1,\*</sup>, Hirokazu Tahara<sup>2</sup>, Nanako Igarashi<sup>3</sup>, Yasuhiro Yamada<sup>3</sup>, and Yoshihiko Kanemitsu<sup>2,†</sup>

<sup>1</sup>Graduate School of Education, Joetsu University of Education, Joetsu, Niigata 943-8512, Japan

<sup>2</sup>Institute for Chemical Research, Kyoto University, Uji, Kyoto 611-011, Japan

<sup>3</sup>Graduate School of Science, Chiba University, Inage, Chiba 263-8522, Japan

 (Received 29 April 2020; revised 22 December 2020; accepted 22 January 2021; published 4 February 2021)

We characterized the temperature dependence of the complex dielectric susceptibility spectrum of a perovskite  $\text{CH}_3\text{NH}_3\text{PbBr}_3$  single crystal by using heterodyne interference spectroscopy. Owing to a time-domain measurement that is not influenced by incoherent lattice relaxations, we were able to detect a low-energy indirect-gap band. We observed two peaks in the energy region below the exciton transition at the  $R$  point in the imaginary part of the spectrum. The temperature dependences of the energies of these peaks were different from the dependence of the energy of the direct-transition exciton. The trends of both the splitting width and peak intensities can be explained by assuming a Rashba spin-split band.

DOI: [10.1103/PhysRevB.103.L081201](https://doi.org/10.1103/PhysRevB.103.L081201)

Owing to the excellent optoelectronic properties of lead halide perovskites and their relatively easy fabrication [1,2], these materials have been considered advantageous for application to optoelectronic devices, such as solar cells [3,4], photodetectors [5], light-emitting diodes [6], lasers [7,8], light modulators [9,10], and high order harmonic light sources [11]. By thoroughly understanding the electronic structure and the dynamics of carriers and excitons in lead halide perovskites, we can expect that fabrication of high-performance devices becomes possible. In particular, the extremely long carrier lifetimes and diffusion lengths in lead halide perovskites have the potential to greatly improve the performance of devices such as solar cells and photodetectors [12–16].

Regarding the reasons for the presence of carriers with long lifetimes in this material, the polaron effect and the Rashba effect have been raised as possible candidates. Polarons form as a result of the strong electron-phonon interactions in perovskites [17,18], and polaron formation reduces the carrier mobility and recombination rate of electrons and holes [19]. On the other hand, the lifetime can also become longer due to the Rashba effect [20–22] where the strong spin-orbit interactions that originate from the heavy atoms in perovskites, e.g., lead and iodine, lead to the formation of an indirect band to band transition. The latter suppresses the radiative recombination. The Rashba effect in perovskites has been reported for a  $\text{MAPbBr}_3$  ( $\text{MA} = \text{CH}_3\text{NH}_3$ ) single crystal [23] and also for colloidal nanocrystals [24]. However, because the Rashba effect is caused by inversion-symmetry breaking, the actual significance of the Rashba effect for the photocarrier transport and recombination processes in bulk perovskite crystals remains controversial [25]. Precise spectroscopic measurements

of the electronic states near the band edge during photoexcitation are a key to advancing our understanding of the peculiar behaviors and the Rashba band splitting in lead halide perovskites. Besides the origin of the long carrier lifetimes in perovskites, a deep understanding of the Rashba effect in perovskites could provide better insights into spin-related phenomena, exciton fine structures, and spintronic applications [26–32].

In this Letter, we clarify the electronic structure near the band edge of a perovskite  $\text{MAPbBr}_3$  single crystal by using heterodyne interference spectroscopy. Heterodyne interference spectroscopy is a highly sensitive spectroscopic technique that uses an optical pulse pair where the relative phase of the two pulses is synchronously locked [33]. Because the sample response is probed by photocurrent (PC), it is possible to measure the real and imaginary parts of the dielectric susceptibility [34]. By using heterodyne interference spectroscopy, the electronic structure can be directly characterized without influences of incoherent lattice relaxations, since the signal is a result of the interference between the photoexcited states. We find that the dielectric susceptibility spectra of the  $\text{MAPbBr}_3$  single crystal exhibit two peaks on the low-energy side of the band gap when sample temperatures are below  $\sim 250$  K. On the basis of temperature-dependence measurements, we conclude that these peaks are not signals from excitonic states, polarons, or shallow traps. We explain why we consider that they originate from the Rashba spin-split band.

The sample used in this work was a  $\text{MAPbBr}_3$  single crystal that was prepared by the inverse temperature crystallization method [35]. Basic properties of the sample are explained in the Supplemental Material [36]. By using a single crystal instead of a thin polycrystalline film, it is possible to reduce surface light-scattering effects. Furthermore, in the case of measuring the photoluminescence (PL) of a single crystal at low temperatures, emission from impurities or defects is usu-

\*ogawa@juen.ac.jp

†kanemitsu@scl.kyoto-u.ac.jp

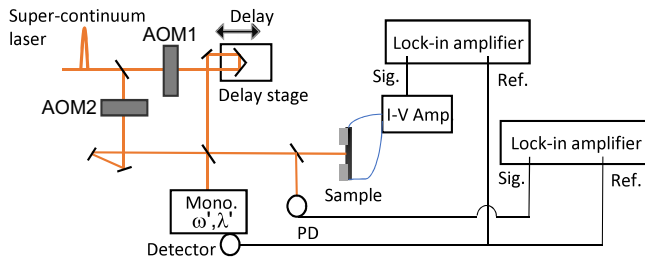


FIG. 1. Experimental setup. AOM: acousto-optic modulator; Mono.: monochromator; PD: photodiode; I-V Amp.: current–voltage amplifier; Sig.: signal; Ref.: reference.

ally observed, which complicates the data analysis. However, by measuring the PC, the free-exciton structure at the band edge can be accurately characterized [37].

As an excitation light source, we used the output beam of a regenerative amplifier (wavelength 800 nm, repetition rate 200 kHz, pulse width 200 fs) pumped by a mode-locked Ti:sapphire laser. Then, by illuminating a sapphire substrate with this excitation beam, we obtained supercontinuum light.

As shown in Fig. 1, the supercontinuum light pulse was passed through a Mach-Zehnder interferometer to generate an optical pulse pair. A delay stage was placed in one of the arms of the interferometer to control the time delay  $\tau$  between the two light pulses. Moreover, an acousto-optic modulator (AOM) was inserted in each arm of the interferometer [33,34]. The two AOMs modulated the frequencies of the pulse pairs by exactly  $\delta\omega_1 = 40.000$  MHz and  $\delta\omega_2 = 40.001$  MHz. Because the frequency shifts differed by 1 kHz, the PC generated by the excitation pulse pair was demodulated by a lock-in amplifier with the 1-kHz reference signal measured by the detector behind the monochromator shown in Fig. 1. An interferogram of the obtained PC signal can be recorded by scanning the time delay  $\tau$ . The details of the analysis method are explained in the Supplemental Material [36].

In Fig. S1(a) in the Supplemental Material [36], we show the interferogram of the PC obtained from the MAPbBr<sub>3</sub> single crystal at 140 K. We used a reference light energy of  $\hbar\omega' = 2.116$  eV, which is smaller than the exciton resonance energy (i.e., the lowest direct optical transition at the *R* point),  $E_0$ .  $E_0$  can be determined from the position of the negative peak in the first derivative of the reflectance (see Fig. S2 in the Supplemental Material [36]). The value obtained here is

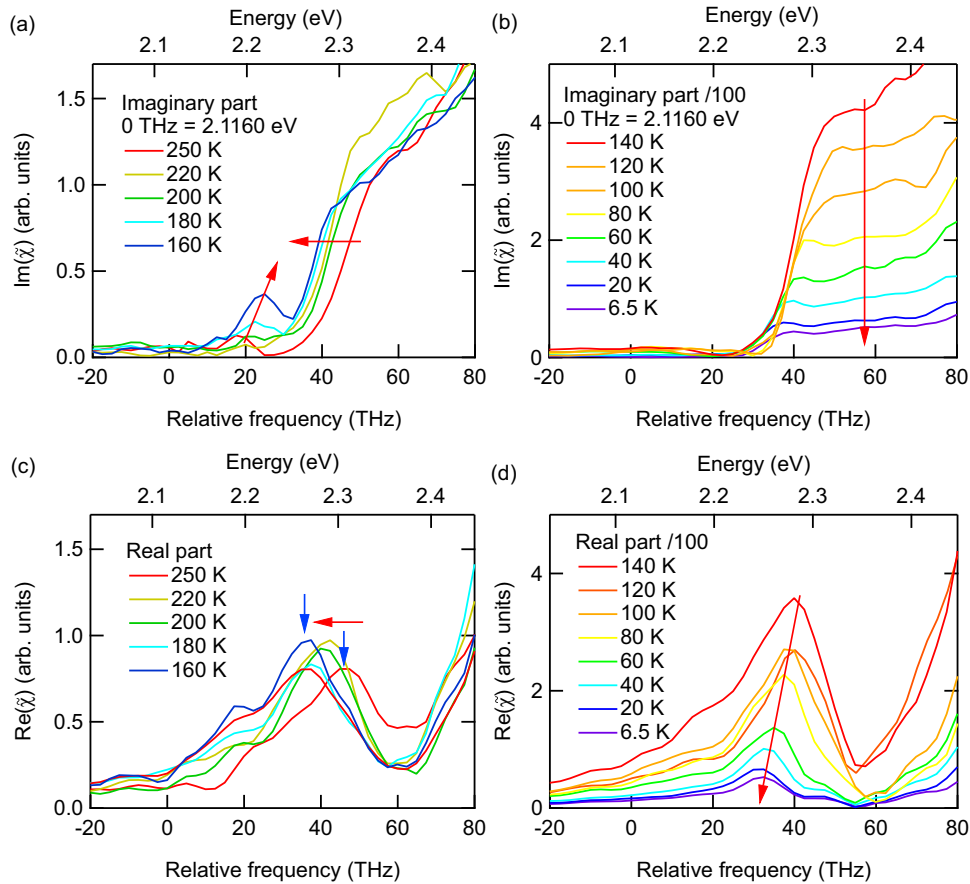


FIG. 2. (a) Temperature dependence of the imaginary part of the dielectric susceptibility,  $\text{Im}(\tilde{\chi})$ , obtained by the Fourier transform of the interferograms in the temperature range from 160 to 250 K. (b) Temperature dependence of  $\text{Im}(\tilde{\chi})$  from 6.5 to 140 K. (c) Temperature dependence of the real part of  $\tilde{\chi}$ ,  $\text{Re}(\tilde{\chi})$ , from 160 to 250 K, and (d) that from 6.5 to 140 K. The red arrows in the figures indicate the peak trends observed for decreasing temperatures. The blue arrows in (c) indicate the peak positions at 250 and 160 K.

consistent with the value reported in the literature [38]. Figure S1(b) shows the interferogram of the excitation pulse pair, which was simultaneously measured by another photodiode, as shown in Fig. 1. The real and imaginary parts of the dielectric susceptibility  $\tilde{\chi}$  are obtained by calculating the integral transform of the PC interferogram [36].

Figure 2 shows the details of the temperature dependence of the spectrum of  $\tilde{\chi}$  of the MAPbBr<sub>3</sub> single crystal. The four separate figures show the real and imaginary parts in two different temperature regimes, because the MAPbBr<sub>3</sub> crystal is tetragonal in the range from  $\sim 160$  to  $\sim 240$  K, and orthorhombic for temperatures below  $\sim 160$  K [39]. As shown in Figs. 2(a) and 2(b), the imaginary part of  $\tilde{\chi}$  has its onset near  $E_0$  ( $E_0 \approx 2.3$  eV at 160 K), and we can see two peaks at around 2.2 eV in Fig. 2(a). Note that these data correspond to the absorption spectra, but owing to the coherent detection technique they exhibit additional features: The peak structures are not observed in the absorption spectrum. (The absorption coefficient at around 2.2 eV is less than  $10^2$  cm<sup>-1</sup>.) Figures 2(c) and 2(d) present the real part of the dielectric susceptibility. The spectra show a peak at the absorption edge, and they match the shape of the real part of  $\tilde{\chi}$  calculated from the results of ellipsometry measurements [40].

Figure 3(a) plots the temperature dependence of the total PC generated by excitation with the pulse pair for  $\tau = 0$  ps. The signal intensity in the orthorhombic phase is two orders of magnitude larger than that in the tetragonal phase. This is attributed to the increase in the mobility of the photocarriers by the structural phase transition from tetragonal phase to orthorhombic phase [41,42]. However, in the tetragonal and orthorhombic phases, the PC signal intensity decreases with decreasing temperature. This trend cannot be explained by the temperature dependence of the carrier mobility. As shown later, this temperature dependence can be interpreted as an increase in the radiative recombination rate as the temperature decreases.

In the following, we focus on the peaks in the energy region below  $E_0$  in Fig. 2(a). Figure 3(b) shows the data at 250 and 160 K together with fitting results. We identified two peaks, hereafter referred to as peak A and peak B. In addition, a weak direct optical transition exists in the energy region below  $E_0$ . The blue arrows in Fig. 3(b) correspond to the peak energies in Fig. 2(c). To evaluate the energy of the weak direct transition,  $E_D$ , the peak in Fig. 2(c) was fitted by using a Lorentzian function, because the real part of  $\tilde{\chi}$  has an extremum at the onset of the direct optical transition [43]. As summarized in Fig. 3(c), both  $E_0$  and  $E_D$  shift towards lower energies as the temperature decreases [44,45]. On the other hand, the energies of peaks A and B,  $E_A$  and  $E_B$ , shift to higher energies as the temperature decreases. Here, we obtained  $E_A$  and  $E_B$  by fitting two Gaussian functions to the peaks, as shown in Fig. 3(b). Additionally, we were not able to clearly observe peaks A and B in the orthorhombic phase [Fig. 2(b)]. We consider that, in the orthorhombic phase, the peaks merge with the band edge, since here the energy difference is smaller.

We can consider several origins for peaks A and B. The first possibility is an exciton-related transition, such as that of a biexciton, bound exciton, or exciton-exciton scattering [46,47]. These transitions appear in the energy region below  $E_0$ . Because the temperature dependences of the binding en-

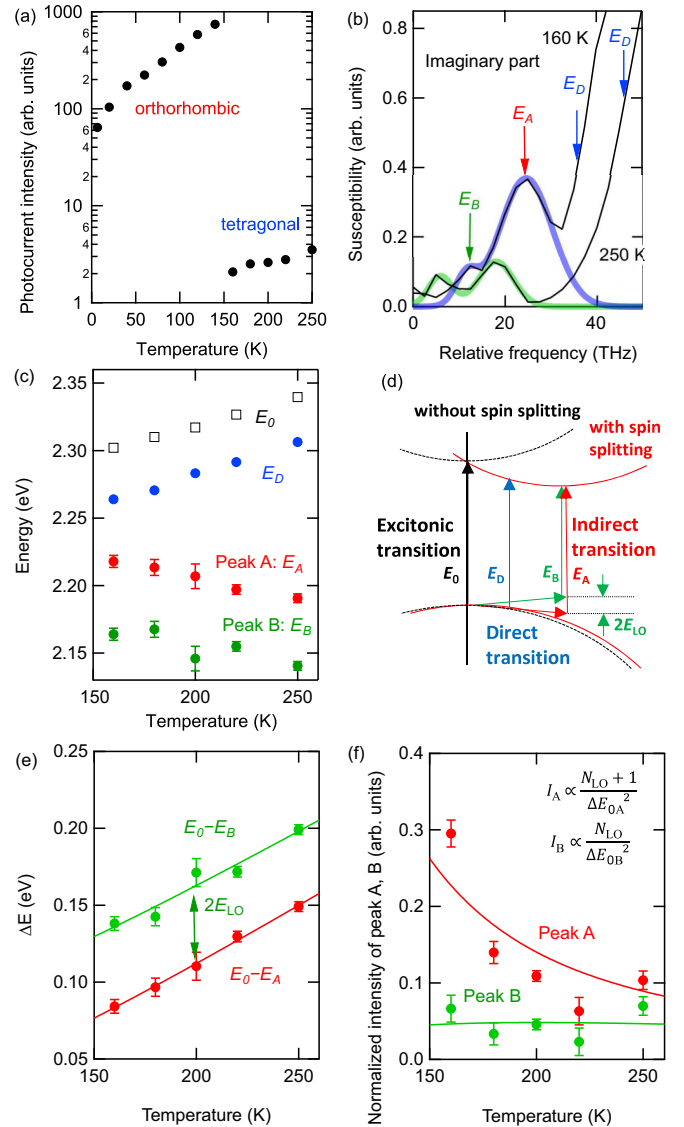


FIG. 3. (a) Temperature dependence of the total PC generated by excitation with the supercontinuum pulses at a delay time of 0 ps. (b) Fitting results for the imaginary part of the dielectric susceptibility at 160 and 250 K (for other temperatures, see Fig. S3 in the Supplemental Material [36]). (c) Temperature dependences of the direct transition energy ( $E_D$ , blue closed circles), the excitonic resonance energy ( $E_0$ , black open squares) which corresponds to the direct transition energy at the  $R$  point, the energy of peak A ( $E_A$ , red closed circles), and peak B ( $E_B$ , green closed circles). (d) Schematic diagram of the Rashba spin-split bands and the optical transition energies,  $E_0$ ,  $E_D$ ,  $E_A$ , and  $E_B$ .  $E_D$  is the direct transition between the Rashba spin-split bands at the point where the conduction and valence bands are parallel to each other. The initial state of the indirect transition is the valence band maximum with a spin-splitting (thus it is different from the  $R$  point). (e) Temperature dependences of the splitting energy ( $\Delta E$ ). (f) Temperature dependences of the intensities of peaks A and B normalized by total PC signal at a delay time of 0 ps.

ergies are usually not very large [48,49], it can be considered that these transition energies will shift towards lower energies in the same way as  $E_0$  does as the temperature decreases. Consequently, it is unlikely that exciton-related transitions

are responsible for peaks *A* and *B*. Transitions due to surface states [50,51], shallow traps, and defects [52], or mixtures of different phases [53], are not plausible origins either, because they exhibit temperature changes similar to the one of  $E_0$ .

Another possible origin is the polaron effect [54]. Large polarons have been observed in several experiments. The temperature dependences of the binding energy and signal intensity of the large polaron are different from those observed for peaks *A* and *B* [55]. Consequently, the large polaron is not a reasonable explanation for the origin of these peaks. Furthermore, for MAPbBr<sub>3</sub> it has been reported that the formation time of large polarons is 0.3 ps [19]. We can conclude that large polarons were not observed in our experiment, because the coherence disappears during the polaron formation (see Fig. S1(a) in the Supplemental Material [36]).

Considering the above discussion, the Rashba effect can be regarded as the most plausible origin of peaks *A* and *B*. The existence of the Rashba effect has been proposed in several theoretical investigations, and its influence on the optical properties has been discussed [20,56,57]. As illustrated in Fig. 3(d), due to the Rashba effect both the valence band and the conduction band split into two spin-polarized bands. Note that the splitting of the conduction band is considered to be larger [20,56]. Therefore, a material with bands that have been split by the Rashba effect exhibits indirect band-gap transitions. In several previous reports, a peak similar to peak *A* was observed on the low-energy side of  $E_D$ , and time-resolved PL measurements have indicated the possibility that this peak is an indirect band to band transition [58,59]. On the other hand, a detailed measurement of PL spectra has revealed that the radiative recombination rate increases when the temperature decreases, which is opposite to what is expected for three-dimensional Rashba semiconductors [25]. Therefore, it is actively debated whether the optical band gap is direct or indirect.

There are two possible ways to break the spatial inversion symmetry: static symmetry breaking due to surfaces and defects, and dynamic symmetry breaking due to thermal fluctuations of the lattice such as those induced by the motion of the organic cation [20,56,57]. Note that with lowering the symmetry of the crystal, the rotation of the MA cation is suppressed, but in the tetragonal phase the MA cation exhibits a threefold rotation mode [60]. It has been reported that the thermal fluctuation of the Pb-Br cage mode can also cause a dynamic Rashba effect [59]. Furthermore, lead halide perovskites have halide vacancies and defects [61,62], and they induce local symmetry breaking and a static local electric field.

The temperature dependences of the splitting widths between  $E_0$  and the peak energies in Fig. 3(c) are shown in Fig. 3(e) as the red ( $\Delta E = E_0 - E_A$ ) and green ( $\Delta E = E_0 - E_B$ ) curves; for both curves, the splitting width  $\Delta E$  increases as the temperature increases. Both curves exhibit the same inclination and their offset is almost constant within the measurement error. From this temperature dependence, we expect that dynamic symmetry breaking is one of the origins of the presently observed Rashba effect [23,59]. To perform a fit of the data, we assumed that the splitting width  $\Delta E$  depends on the phonon population; the fitting result obtained using the Bose distribution function  $\Delta E = \Delta E_0 +$

$A/[\exp(E_{LO}/k_B T) - 1]$  is shown with the solid curves. Here,  $E_{LO}$  is the literature value of the longitudinal optical (LO) phonon energy (20.1 meV) [63], and we used it as a constant.  $\Delta E_0$  is the temperature-independent term,  $k_B$  is the Boltzmann constant, and  $A$  is a normalization constant. Because the fitting curves agree well with the experimental curves, we conclude that the splitting width  $\Delta E$  originates from the LO phonon. The parameters obtained from the fitting procedure are  $A = 192 \pm 7(179 \pm 26)$  meV and  $\Delta E_0 = 25 \pm 3(81 \pm 12)$  meV for peak *A* (*B*).

As can be seen in Fig. 3(b), the intensity of peak *A* increases with decreasing temperature while that of peak *B* hardly changes. Because we used PC to probe the sample response, the signal intensity depends on factors such as the mobility of the photocarriers. To remove such influences, we normalized the intensities of peaks *A* and *B* by the total PC in Fig. 3(a). The results are summarized in Fig. 3(f). Considering the fact that the transitions in Fig. 3(b) have a well-defined peak structure, it can be considered that the indirect transitions to the conduction band minima [Fig. 3(d), absorption process indicated with red and green arrows] have a high probability. The dynamic Rashba effect is caused by thermal fluctuations of the MA cation and the Pb-Br cage mode, where the fluctuations occur on the 100-fs timescale [56,64]. Therefore, we can observe the interference signal when the spin-split is the strongest, because the position of the MA cation and the Pb-Br is the most displaced at that time and the behavior of the motion is almost stationary during the measurement. Furthermore, under the condition  $\hbar\omega = E_A$ , only the conduction band minimum is involved in the generation of the interference signal. This signal becomes weaker for  $E_D > \hbar\omega > E_A$ , since here multiple final states are excited because there are multiple transition processes using LO phonons with different momenta. This mechanism is responsible for the signal peak at the indirect band edge. We consider that peaks *A* and *B* correspond to phonon emission (Stokes) and absorption (anti-Stokes) processes, because we found that  $E_A - E_B \approx 2E_{LO}$ , independent of temperature as shown in Fig. 3(e). It should be possible to describe the intensities of the normalized peaks by  $I_A \propto (N_{LO} + 1)/\Delta E'^2$  and  $I_B \propto N_{LO}/\Delta E'^2$ , where  $N_{LO}$  is the LO phonon occupation number and  $\Delta E' = E_{i0} - \hbar\omega$ .  $E_{i0}$  is the energy difference between the initial  $|0\rangle$  and intermediate  $|i\rangle$  states in the photon absorption process [43]. We fitted the data by assuming that  $\Delta E' \sim E_0 - E_A$  for  $I_A$  and  $\Delta E' \sim E_0 - E_B$  for  $I_B$ . The obtained fitting results are shown with the solid curves in Fig. 3(f). Because the predicted trend agrees fairly well with the experimental results, we conclude that peaks *A* and *B* are indirect transitions to the spin-split band. The intensity of peak *A* increases because the photoabsorption process approaches the resonance condition. Note that, in this temperature region, the contribution of  $N_{LO}$  to the temperature dependence of the peak intensity is small compared to that of the resonance condition. The temperature dependences of the peak intensities in Fig. 3(f) cannot be explained by bound excitons, polarons, and shallow traps. Only the Rashba effect can quantitatively explain these temperature dependences.

The average value of the temperature-independent term  $\Delta E_0$  for peaks *A* and *B* is  $53 \pm 8$  meV. This value presents the energy shift due to the static Rashba effect. By using this value, we can estimate the energy shift due to the

dynamic Rashba effect: We obtain 121 meV at 250 K and 58 meV at 160 K. At high temperatures near room temperature, the contribution of the dynamic Rashba effect is larger than that of the static one, but the oscillator strength of the indirect transition is extremely small compared with that of the direct optical transition at the  $R$  point. Considering the significantly smaller oscillator strength of optical transition involving the Rashba split band, it is likely that the Rashba effect observed here is only determined by a limited volume. Moreover, electron-phonon interactions, which are particularly important in perovskites, form large polarons [19,54,55]. Thus, it is difficult to observe the Rashba splitting band in the conventional PL and absorption measurements. On the other hand, at low temperatures where the oscillator strength of the indirect transition becomes stronger, the contribution of the static Rashba effect is rather dominant compared with the dynamic Rashba and polaron effects.

In conclusion, we have presented the complex dielectric susceptibility spectra of a MAPbBr<sub>3</sub> single crystal at different

temperatures. In the imaginary part of the dielectric susceptibility spectra, two peaks appeared on the low-energy side of the direct optical transition, and their intensities were much smaller than the intensity of the direct transition at the  $R$  point. The temperature dependence of the splitting width between each peak energy and the excitonic transition at the  $R$  point matched the dependence predicted by using the LO phonon occupation number. Moreover, the temperature dependences of the signal intensities of two peaks indicated that the peaks are indirect transitions. Based on the above results, we concluded that the peaks at the low-energy side of the band gap are indirect transitions to the Rashba spin-split band.

This work was supported by the International Collaborative Research Program of the Institute for Chemical Research, Kyoto University (Grant No. 2019-28). Part of this work was supported by JSPS KAKENHI Grant No. JP16K05399 (to Y.O.) and JSPS KAKENHI Grant-in-Aid for Specially Promoted Research Grant No. JP19H05465 (to Y.K.).

- 
- [1] S. D. Stranks and H. J. Snaith, *Nat. Nanotechnol.* **10**, 391 (2015).
- [2] Y. Kanemitsu, *J. Mater. Chem. C* **5**, 3427 (2017).
- [3] A. Kojima, K. Teshima, Y. Shirai, and T. Miyasaka, *J. Am. Chem. Soc.* **131**, 6050 (2009).
- [4] M. M. Lee, J. Teuscher, T. Miyasaka, T. N. Murakami, and H. J. Snaith, *Science* **338**, 643 (2012).
- [5] L. Dou, Y. Yang, J. You, Z. Hong, W.-H. Chang, G. Li, and Y. Yang, *Nat. Commun.* **5**, 5404 (2014).
- [6] Z.-K. Tan, R. S. Moghaddam, M. L. Lai, P. Docampo, R. Higler, F. Deschler, M. Price, A. Sadhanala, L. M. Pazos, and D. Credgington, *Nat. Nanotechnol.* **9**, 687 (2014).
- [7] G. Xing, N. Mathews, S. S. Lim, N. Yantara, X. Liu, D. Sabba, M. Grätzel, S. Mhaisalkar, and T. C. Sum, *Nat. Mater.* **13**, 476 (2014).
- [8] H. Zhu, Y. Fu, F. Meng, X. Wu, Z. Gong, Q. Ding, M. V. Gustafsson, M. T. Trinh, S. Jin, and X.-Y. Zhu, *Nat. Mater.* **14**, 636 (2015).
- [9] H. Tahara, T. Aharen, A. Wakamiya, and Y. Kanemitsu, *Adv. Opt. Mater.* **6**, 1701366 (2018).
- [10] T. Handa, H. Tahara, T. Aharen, and Y. Kanemitsu, *Sci. Adv.* **5**, eaax0786 (2019).
- [11] H. Hirori, P. Xia, Y. Shinohara, T. Otobe, Y. Sanari, H. Tahara, N. Ishii, J. Itatani, K. L. Ishikawa, T. Aharen, M. Ozaki, A. Wakamiya, and Y. Kanemitsu, *APL Mater.* **7**, 041107 (2019).
- [12] S. D. Stranks, G. E. Eperon, G. Grancini, C. Menelaou, M. J. P. Alcocer, T. Leijtens, L. M. Herz, A. Petrozza, and H. J. Snaith, *Science* **342**, 341 (2013).
- [13] G. Xing, N. Mathews, S. Sun, S. S. Lim, Y. M. Lam, M. Grätzel, S. Mhaisalkar, and T. C. Sum, *Science* **342**, 344 (2013).
- [14] D. Shi, V. Adinolfi, R. Comin, M. Yuan, E. Alarousu, A. Buin, Y. Chen, S. Hoogland, A. Rothenberger, and K. Katsiev, *Science* **347**, 519 (2015).
- [15] Y. Yamada, T. Nakamura, M. Endo, A. Wakamiya, and Y. Kanemitsu, *J. Am. Chem. Soc.* **136**, 11610 (2014).
- [16] Y. Bi, E. M. Hutter, Y. Fang, Q. Dong, J. Huang, and T. J. Savenije, *J. Phys. Chem. Lett.* **7**, 923 (2016).
- [17] X.-Y. Zhu and V. Podzorov, *J. Phys. Chem. Lett.* **6**, 4758 (2015).
- [18] Y. Yamada, H. Mino, T. Kawahara, K. Oto, H. Suzuura, and Y. Kanemitsu, *arXiv:2001.07901*.
- [19] K. Miyata, D. Meggiolaro, M. T. Trinh, P. P. Joshi, E. Mosconi, S. C. Jones, and X.-Y. Zhu, *Sci. Adv.* **3**, e1701217 (2017).
- [20] F. Zheng, L. Z. Tan, S. Liu, and A. M. Rappe, *Nano Lett.* **15**, 7794 (2015).
- [21] M. Kepenekian, R. Robles, C. Katan, D. Saporì, L. Pedesseau, and J. Even, *ACS Nano* **9**, 11557 (2015).
- [22] Z.-G. Yu, *Phys. Chem. Chem. Phys.* **19**, 14907 (2017).
- [23] D. Niesner, M. Wilhelm, I. Levchuk, A. Osvet, S. Shrestha, M. Batentschuk, C. Brabec, and T. Fauster, *Phys. Rev. Lett.* **117**, 126401 (2016).
- [24] M. Isarov, L. Z. Tan, M. I. Bodnarchuk, M. V. Kovalenko, A. M. Rappe, and E. Lifshitz, *Nano Lett.* **17**, 5020 (2017).
- [25] V. Sarritzu, N. Sestu, D. Marongiu, X. Chang, Q. Wang, S. Masi, S. Colella, A. Rizzo, A. Gocalinska, E. Pelucchi, M. L. Mercuri, F. Quochi, M. Saba, A. Mura, and G. Bongiovanni, *Adv. Opt. Mater.* **6**, 1701254 (2018).
- [26] D. Niesner, M. Hauck, S. Shrestha, I. Levchuk, G. J. Matt, A. Osvet, M. Batentschuk, C. Brabec, H. B. Weber, and T. Fauster, *Proc. Natl. Acad. Sci. USA* **115**, 9509 (2018).
- [27] P. Odenthal, W. Talmadge, N. Gundlach, R. Wang, C. Zhang, D. Sun, Z.-G. Yu, Z. V. Vardeny, and Y. S. Li, *Nat. Phys.* **13**, 894 (2017).
- [28] P. A. Obraztsov, D. Lyashenko, P. A. Chizhov, K. Konishi, N. Nemoto, M. Kuwata-Gonokami, E. Welch, A. N. Obraztsov, and A. Zakhidov, *Commun. Phys.* **1**, 14 (2018).
- [29] X. Liu, A. Chanana, U. Huynh, F. Xue, P. Haney, S. Blair, X. Jiang, and Z. V. Vardeny, *Nat. Commun.* **11**, 323 (2020).
- [30] J. Li and P. M. Haney, *Appl. Phys. Lett.* **109**, 193903 (2016).
- [31] M. A. Becker, R. Vaxenburg, G. Nedulcu, P. C. Sercel, A. Shabaev, M. J. Mehl, J. G. Michopoulos, S. G. Lambrakos, N. Bernstein, J. L. Lyons, T. Stöferle, R. F. Mahrt, M. V.

- Kovalenko, D. J. Norris, G. Rainò, and A. L. Efros, *Nature* **553**, 189 (2018).
- [32] P. Tamarat, M. I. Bodnarchuk, J.-B. Trebbia, R. Erni, M. V. Kovalenko, J. Even, and B. Lounis, *Nat. Mater.* **18**, 717 (2019).
- [33] Y. Ogawa, *Phys. Rev. B* **95**, 201113(R) (2017).
- [34] P. F. Tekavec, T. R. Dyke, and A. H. Marcus, *J. Chem. Phys.* **125**, 194303 (2006).
- [35] M. I. Saidaminov, A. L. Abdelhady, B. Murali, E. Alarousu, V. M. Burlakov, W. Peng, I. Dursun, L. Wang, Y. He, G. Maculan, A. Goriely, T. Wu, O. F. Mohammed, and O. M. Bakr, *Nat. Commun.* **6**, 7586 (2015).
- [36] See Supplemental Material at <http://link.aps.org/supplemental/10.1103/PhysRevB.103.L081201> for details of the analysis of photocurrent data obtained by heterodyne interference spectroscopy, basic material properties, and the assignment of the peaks in the imaginary part of the dielectric susceptibility.
- [37] L. Q. Phuong, Y. Nakaike, A. Wakamiya, and Y. Kanemitsu, *J. Phys. Chem. Lett.* **7**, 4905 (2016).
- [38] Y. Guo, O. Yaffe, T. D. Hull, J. S. Owen, D. R. Reichman, and L. E. Brus, *Nat. Commun.* **10**, 1175 (2019).
- [39] N. Onoda-Yamamoto, T. Matsuo, and H. Suga, *J. Phys. Chem. Solids* **53**, 935 (1992).
- [40] A. M. A. Leguy, P. Azarhoosh, M. I. Alonso, M. Campoy-Quiles, O. J. Weber, J. Yao, D. Bryant, M. T. Weller, J. Nelson, A. Walsh, M. van Schilfgaarde, and P. R. F. Barnes, *Nanoscale* **8**, 6317 (2016).
- [41] H. T. Yi, X. Wu, X.-Y. Zhu, and V. Podzorov, *Adv. Mater.* **28**, 6509 (2016).
- [42] M. C. Gelvez-Rueda, D. H. Cao, S. Patwardhan, N. Renaud, C. C. Stoumpos, G. C. Schatz, J. T. Hupp, O. K. Farha, T. J. Savenije, M. G. Kanatzidis, and F. C. Grozema, *J. Phys. Chem. C* **120**, 16577 (2016).
- [43] P. Y. Yu and M. Cardona, *Fundamentals of Semiconductors* (Springer, Berlin, 2010).
- [44] B. J. Foley, D. L. Marlowe, K. Sun, W. A. Saidi, and L. Scudiero, *Appl. Phys. Lett.* **106**, 243904 (2015).
- [45] L.-Y. Huang and W. R. L. Lambrecht, *Phys. Rev. B* **88**, 165203 (2013).
- [46] H. Kunugita, Y. Kiyota, Y. Udagawa, Y. Takeoka, Y. Nakamura, J. Sano, T. Matsushita, T. Kondo, and K. Ema, *Jpn. J. Appl. Phys.* **55**, 060304 (2016).
- [47] Y. H. Qiu, F. Nan, Q. Wang, X.-D. Liu, S.-J. Ding, Z.-H. Hao, L. Zhou, and Q.-Q. Wang, *J. Phys. Chem. C* **121**, 6916 (2017).
- [48] Y. Yamada, T. Nakamura, M. Endo, A. Wakamiya, and Y. Kanemitsu, *IEEE J. Photovoltaics* **5**, 401 (2015).
- [49] K. Galkowski, A. Mitioglu, A. Miyata, P. Plochocka, O. Portugall, G. E. Eperon, J. T. Wang, T. Stergiopoulos, S. D. Stranks, H. J. Snaith, and R. J. Nicholas, *Energy Environ. Sci.* **9**, 962 (2016).
- [50] B. Wu, H. T. Nguyen, Z. Ku, G. Han, D. Giovanni, N. Mathews, H. J. Fan, and T. C. Sum, *Adv. Energy Mater.* **6**, 1600551 (2016).
- [51] B. Murali, S. Dey, A. L. Abdelhady, W. Peng, E. Alarousu, A. R. Kirmani, N. Cho, S. P. Sarmah, M. R. Parida, M. I. Saidaminov, A. A. Zhumekenov, J. Sun, M. S. Alias, E. Yengel, B. S. Ooi, A. Amassian, O. M. Bakr, and O. F. Mohammed, *ACS Energy Lett.* **1**, 1119 (2016).
- [52] Z. Ni, C. Bao, Y. Liu, Q. Jiang, W.-Q. Wu, S. Chen, X. Dai, B. Chen, B. Hartweg, Z. Yu, Z. Holman, and J. Huang, *Science* **367**, 1352 (2020).
- [53] L. Q. Phuong, Y. Yamada, M. Nagai, N. Maruyama, A. Wakamiya, and Y. Kanemitsu, *J. Phys. Chem. Lett.* **7**, 2316 (2016).
- [54] D. Emin, *J. Appl. Phys.* **123**, 055105 (2018).
- [55] K. T. Munson, E. R. Kennehan, G. S. Doucette, and J. B. Asbury, *Chem* **4**, 2826 (2016).
- [56] E. Mosconi, T. Etienne, and F. De Angelis, *J. Phys. Chem. Lett.* **8**, 2247 (2017).
- [57] T. Etienne, E. Mosconi, and F. De Angelis, *J. Phys. Chem. Lett.* **7**, 1638 (2016).
- [58] T. Wang, B. Daiber, J. M. Frost, S. A. Mann, E. C. Garnett, A. Walsh, and B. Ehrler, *Energy Environ. Sci.* **10**, 509 (2017).
- [59] B. Wu, H. Yuan, Q. Xu, J. A. Steele, D. Giovanni, P. Pucel, J. Fu, Y. F. Ng, N. F. Jamaludin, A. Solanki, S. Mhaisalkar, N. Mathews, M. B. J. Roeffaers, M. Grätzel, J. Hofkens, and T. C. Sum, *Nat. Commun.* **10**, 484 (2019).
- [60] T. Chen, B. J. Foley, B. Ipek, M. Tyagi, J. R. D. Copley, C. M. Brown, J. J. Choi, and S.-H. Lee, *Phys. Chem. Chem. Phys.* **17**, 31278 (2015).
- [61] H. Huang, M. I. Bodnarchuk, S. V. Kershaw, M. V. Kovalenko, and A. L. Rogach, *ACS Energy Lett.* **2**, 2071 (2017).
- [62] D. P. Nenon, K. Pressler, J. Kang, B. A. Koscher, J. H. Olshansky, W. T. Osowiecki, M. A. Koc, L. Wang, and A. P. Alivisatos, *J. Am. Chem. Soc.* **140**, 17760 (2018).
- [63] M. Nagai, T. Tomioka, M. Ashida, M. Hoyano, R. Akashi, Y. Yamada, T. Aharen, and Y. Kanemitsu, *Phys. Rev. Lett.* **121**, 145506 (2018).
- [64] O. Yaffe, Y. Guo, L. Z. Tan, D. A. Egger, T. Hull, C. C. Stoumpos, F. Zheng, T. F. Heinz, L. Kronik, M. G. Kanatzidis, J. S. Owen, A. M. Rappe, M. A. Pimenta, and L. E. Brus, *Phys. Rev. Lett.* **118**, 136001 (2017).